Redox Biology 62 (2023) 102679

Contents lists available at ScienceDirect

Redox Biology

journal homepage: www.elsevier.com/locate/redox

TRIM21 deficiency protects against atrial inflammation and remodeling post myocardial infarction by attenuating oxidative stress

Xiangdong Liu [1], Wenming Zhang [1], Jiachen Luo, Wentao Shi, Xingxu Zhang, Zhiqiang Li, Xiaoming Qin, Baoxin Liu [**], Yidong Wei [*]

Department of Cardiology, Shanghai Tenth People's Hospital, Tongji University School of Medicine, 301 Middle Yanchang Road, Shanghai, 200072, China

ARTICLE INFO

Keywords:
Tripartite motif-containing protein 21
Myocardial infarction
Oxidative stress
Inflammation
Nuclear factor kappa B
NADPH oxidase 2

ABSTRACT

Atrial remodeling is a major contributor to the onset of atrial fibrillation (AF) after myocardial infarction (MI). Tripartite motif-containing protein 21 (TRIM21), an E3 ubiquitin protein ligase, is associated with pathological cardiac remodeling and dysfunction. However, the role of TRIM21 in postmyocardial infarction atrial remodeling and subsequent AF remains unclear. This study investigated the role of TRIM21 in post myocardial infarction atrial remodeling using TRIM21 knockout mice and explored the underlying mechanisms by overexpressing TRIM21 in HL-1 atrial myocytes using a lentiviral vector. The expression of TRIM21 in the left atrium of the mouse MI model was significantly elevated. TRIM21 deficiency alleviated MI-induced atrial oxidative damage, Cx43 downregulation, atrial fibrosis and enlargement, and abnormalities in electrocardiogram parameters (prolongation of the P-wave and PR interval). TRIM21 overexpression in atrial myocyte HL-1 cells further enhanced oxidative damage and Cx43 downregulation, whereas these effects were reversed by the reactive oxygen species scavenger N-acetylcysteine. The findings suggest that TRIM21 likely induces Nox2 expression mechanistically by activating the NF-κB pathway, which in turn leads to myocardial oxidative damage, inflammation, and atrial remodeling.

1. Introduction

Atrial fibrillation (AF) is the most common form of arrhythmia in patients with acute myocardial infarction (MI), with an incidence of 6.8–21% [1,2]. Patients with AF post-MI are at a heightened risk of worse clinical outcomes and mortality than patients without AF post-MI [3,4]. However, the fundamental mechanism linking MI to the development of AF remains unclear. Structural and electrical remodeling of the atria are prerequisites for the development of AF [5]. Several factors are involved in atrial remodeling post-MI, including ischemia, stretching, alterations in the autonomic nervous system, and inflammation [6].

Emerging evidence demonstrates that oxidative stress plays a critical role in the pathogenesis of AF following MI. Plasma markers of oxidative stress were elevated in patients with ST elevation MI and were associated with the initiation of AF[7]. An imbalance between the production of reactive oxygen species (ROS) and antioxidant activity is the primary cause of oxidative stress [8]. Nicotinamide adenine dinucleotide phosphate (NADPH) oxidase (NOX) is the main contributor to intracellular ROS production in MI-induced myocardial injury [9]. In human atrial myocytes, superoxide is mainly produced by Nox2, which is significantly upregulated in atrial tissues from animal models and patients with AF [10,11]. Knockdown of Nox2 in the atrium of dogs alleviates rapid pacing-induced atrial myocyte oxidative injury and reduces AF inducibility [12]. Additionally, increased expression of Nox2 in atrial myocytes has been linked to the degree of atrial remodeling in patients with mitral regurgitation [13]. Based on the above findings, it is speculated that Nox2 may play an important role in atrial remodeling following MI.

Tripartite motif-containing protein 21 (TRIM21), an E3 ubiquitin ligase, plays an essential role in regulating cellular processes, such as redox homeostasis, transcription, apoptosis, autophagy, and

Abbreviations: AF, Atrial fibrillation; BSA, Bovine serum albumin; DMEM, Dulbecco's Modified Eagle's Medium; H&E, Hematoxylin and eosin; LA, Left atrial; LAD, Left anterior descending; MI, Myocardial infarction; MOI, Multiplicities of infection; ROS, Reactive oxygen species; TAC, Transverse aortic constriction; TL, Tibia length; SD, Standard deviations.

* Corresponding author.
** Corresponding author.
E-mail addresses: wfboys@163.com (B. Liu), ywei@tongji.edu.cn (Y. Wei).
[1] These two authors contributed equally to this work.

https://doi.org/10.1016/j.redox.2023.102679
Received 7 February 2023; Received in revised form 5 March 2023; Accepted 15 March 2023
Available online 22 March 2023

inflammation [14,15]. TRIM21 is widely expressed in various tissues but is particularly enriched in the heart and immune system [16,17]. Accumulating evidence suggests that TRIM21 is involved in the development of cardiovascular diseases. For example, TRIM21 protects mice from CVB3 viral-induced myocarditis by enhancing the interferon regulatory factor 3-mediated type I interferon signaling pathway [18]. TRIM21 knockout (KO) attenuates transverse aortic constriction (TAC)-induced ventricular myocyte oxidative damage, thereby protecting cardiac systolic function [16]. However, it remains unclear whether TRIM21 regulates atrial remodeling following MI.

This study aimed to explore the role of TRIM21 in atrial remodeling following MI and to identify whether Nox2 is an essential downstream effector molecule in this process.

2. Methods

2.1. Experimental animals

The generation of homozygous TRIM21 knockout (KO) mice has been described in our previous study [19]. Animal experiments were carried out according to the Chinese National Institutes of Health and Animal Care guidelines and were approved by the Animal Care Ethics Committee of Shanghai Tenth People's Hospital of Tongji University School of Medicine (approval number: SHDSYY-2020-1734). Mice were housed in a humidity- and temperature-controlled environment with controlled light cycles (12-h light and 12-h dark).

2.2. Animal grouping and the MI model

Age- (8–10 weeks) and weight- (20–25 g) matched male mice were randomly assigned to the following four groups: wild-type sham group (WT-Sham), wild-type mice without left anterior descending branch (LAD) ligation; TRIM21 knockout sham group (KO-Sham), TRIM21 knockout mice without LAD ligation; wild-type MI group (WT-MI), wild-type mice with LAD ligation, and TRIM21 knockout MI group (KO-MI), TRIM21 knockout mice with LAD ligation.

The mouse MI model was established according to a previous report [20]. Briefly, mice were anesthetized with a 2% isoflurane inhalation oxygen mixture without intubation. An incision of 1–2 cm was made to expose the fourth intercostal space, the heart was carefully squeezed out of the thoracic cavity, and the LAD was smoothly secured using a silk (6–0) suture slipknot. Whitening of the left ventricular anterior wall was considered an indication of successful induction of myocardial ischemia. The mouse heart was then instantly repositioned into the chest, air and blood were squeezed out, and the chest was sutured. The sham mice underwent the same surgery, but the LAD artery was not tied.

2.3. Echocardiography analysis

Left atrial (LA) size was measured using echocardiography 4 weeks after infarct induction. Briefly, mice were lightly anesthetized with 1.5%–2% isoflurane to maintain spontaneous breathing. Echocardiography was performed using an 18–30 MHz transducer with a Vevo 2100 system (VisualSonics, Toronto, Canada). LA area was performed in parasternal long-axis views using m-mode or two-dimensional echocardiography. Peak velocity of the early ventricular filling (E wave) and peak velocity of the late ventricular filling (A wave) were acquired from the apical four-chamber view.

2.4. Electrocardiograph analysis

The mice were lightly anesthetized with 1.5%–2% isoflurane without intubation. Lead II electrocardiography (ECG) was performed using a biological signal acquisition system (BL-420S, Chengdu, China). The ECG waveforms from four consecutive heartbeats were averaged and analyzed using LabChart 7 Pro software (AD Instruments, Sydney, Australia).

2.5. Masson trichrome and hematoxylin and eosin (H&E) staining

Paraffin-embedded mouse LA specimens were fixed in paraformaldehyde and sectioned at a thickness of 4 μm. A Masson's trichrome staining kit (Solarbio, Beijing, China) was used to assess atrial fibrosis, while a hematoxylin and eosin (H&E) staining kit (Solarbio, Beijing, China) was used to evaluate left atrial morphology. All steps were performed according to the manufacturer's instructions. An Olympus IX83 fluorescence microscope (Olympus, Tokyo, Japan) was used to visualize slides. The fibrotic area was measured using ImageJ software (version 1.8.0).

2.6. Cell culture and transfection

HL-1 mouse atrial myocytes were acquired from Procell (Wuhan, China). The cells were cultured in a humidified atmosphere at 37 °C and 5% CO2 in Dulbecco's Modified Eagle's medium (DMEM) (Biological Industries, Bet-Haemek, Israel) supplemented with 10% fetal bovine serum (Biological Industries). GenePharma (Shanghai, China) constructed a TRIM21 overexpression lentiviral vector (Lenti-TRIM21) and a negative control (NC) Lenti-green fluorescent protein (Lenti-GFP) vector. HL-1 cells were transduced with Lenti-GFP and Lenti-TRIM21 at 100 multiplicities of infection (MOI) for 12 h, followed by selection with puromycin. To induce a cellular model of oxidative damage, HL-1 cells were treated with H_2O_2 (150 μM) for 12 h, whereas the control group was treated with PBS. N-acetylcysteine (NAC, MedChemExpress, NJ, USA) was used at a concentration of 5 mM as an ROS inhibitor, and dimethyl sulfoxide (DMSO, Sigma Aldrich, St. Louis, MO, USA) was used as a solvent control. Vas2870 (MedChemExpress) was used at a concentration of 50 μM as a Nox2 inhibitor, while DMSO was used as a control. Bay11–7082 (MedChemExpress) was used at a concentration of 10 μM as an NF-κB pathway inhibitor, with DMSO as a control.

2.7. Immunofluorescence staining

HL-1 cells grown on glass slides and LA tissues were treated with 4% paraformaldehyde for 15 min at ambient temperature and then with 0.1% Triton X-100 for 15 min at 4 °C. Next, the slides and sections were blocked using 5% bovine serum albumin (BSA) for 30 min at ambient temperature and subsequently incubated overnight with primary antibodies against Cx43 (dilution 1:200, ab78055, Abcam), TRIM21 (dilution 1:100, ab232549, Abcam, Cambridge, UK), and MAC-2 (dilution 1:100, sc-374541, Santa Cruz Biotechnology, Santa Cruz, CA) at 4 °C. Subsequently, Alexa Fluor 488/594 fluorophore-labeled secondary antibody (Yeasen Biotechnology, Shanghai, China) was applied to the slides and sections. Apoptotic cells were detected using a terminal deoxynucleotidyl transferase-mediated dUTP nick-end labeling (TUNEL) apoptosis detection kit (Yeasen). All immunofluorescence experiments were performed with the addition of DAPI to stain the nuclei. An Olympus IX83 fluorescence microscope (Olympus, Tokyo, Japan) was used to visualize slides and sections. Six random fields were selected, and the fluorescence intensities were calculated using ImageJ software.

2.8. ROS detection

HL-1 cells were pretreated with NAC, BAY 11–7082 and Vas7820 before exposure to H_2O_2 and then incubated with 10 μM dihydroethidium (DHE) (Yeasen, Shanghai, China) for 20 min, and ROS levels were measured using DHE fluorescence [21,22]. The LA tissue of each mouse was sectioned into 8 μm thick slices and dyed with DHE. Both the slides and sections were visualized using an Olympus IX83 fluorescence microscope (Olympus Corporation) and analyzed using ImageJ software.

2.9. Wheat germ agglutinin (WGA) staining

LA tissues were cut into 5 μm sections at an optimal temperature and then incubated with 5 μM WGA (Thermo, MA, United States) at 37 °C for 30 min. An Olympus IX83 fluorescence microscope (Olympus, Tokyo, Japan) was used to capture the sections, and the surface area was calculated using ImageJ software.

2.10. Western blot analysis

Proteins were isolated from HL-1 cells and LA tissues using radioimmunoprecipitation assay lysis (RIPA) buffer (Beyotime) and quantified using bicinchoninic acid (BCA) reagent (Beyotime). Proteins (20–40 μg) were separated by sodium dodecyl sulfate–polyacrylamide gel electrophoresis (SDS–PAGE) and transferred onto polyvinylidene fluoride (PVDF) membranes (Millipore, Billerica, MA, USA). To prevent nonspecific binding, membranes were blocked with 5% BSA. Membranes were then incubated overnight with primary antibodies at 4 °C. Finally, the membranes were incubated with secondary antibodies and visualized using enhanced chemiluminescence reagents (Shenger Biotechnology, Shanghai, China). The primary antibodies used were as follows: Cx43 (ab78055, Abcam), TRIM21 (ab232549, Abcam), MAC-2 (sc-374253, Santa Cruz), Bcl-2 (3498S, CST), total nuclear factor-κB (t–NF–κB) (T55034, total–NF–κB, Abmart, Shanghai, China), phosphatidylinositol NF-κB (TA2006, p–NF–κB, Abmart), Bax (2772S, CST), Nox2 (abs124860, Absin, Shanghai, China), γ-H2AX (ab81299, Abcam), GAPDH (5174S, CST), collagen I (ab260043, Abcam), α-SMA (ET1607-53, Huabio, Hangzhou, China), and horseradish peroxidase-labeled secondary antibodies (Huabio).

2.11. Quantitative real-time polymerase chain reaction

Total RNA was extracted from HL-1 cells and LA tissues using TRIzol reagent (Takara, Dalian, China). Complementary DNA was synthesized using the PrimeScript RT Reagent Kit (Takara). All subsequent amplifications were conducted using a LightCycler 480 Real-time PCR System (Roche) and Hieff® qPCR SYBR Green Master Mix (No Rox) (Yeasen, Shanghai, China). Target gene expression was quantified using the $2^{-\Delta\Delta Ct}$ method with normalization to GAPDH expression. Primer sequences are provided in Supplementary Table 1.

2.12. Measurement of malondialdehyde (MDA) and superoxide dismutase (SOD)

Samples of cell supernatant and mouse serum from each group were collected to assess the concentrations of malondialdehyde (MDA) and superoxide dismutase (SOD) activity using MDA and SOD kits (Beyotime), according to the manufacturer's instructions.

2.13. Statistical analysis

Data analysis was conducted using GraphPad Prism version 8.0 (GraphPad Software, San Diego, CA). All data are expressed as the mean ± standard deviation (SD). The normality of the data was assessed using the Shapiro–Wilk test. Two-sample comparisons were performed using a two-tailed Student's t-test. For comparisons between multiple groups (≥3 groups), one-way ANOVA followed by Bonferroni post hoc test was performed. Nonparametric data were compared using an unpaired, two-tailed Mann–Whitney test (two groups) or the Kruskal–Wallis with Dunn post hoc test (≥3 groups). Statistical significance was set at $P < 0.05$.

3. Results

3.1. TRIM21 deficiency alleviates LA fibrosis post-MI

Expression of TRIM21 in left atrial tissues of mice was examined first. As shown in Fig. 1a, compared to sham-operated mice, both mRNA and protein expression of TRIM21 increased on day 3 but decreased on day 14 after MI. The expression of TRIM21 protein and mRNA had no significant difference between 14 and 28 days. Consistent with this finding, the fluorescence intensity of TRIM21-positive cells in the LA increased on day 3 but decreased on day 14 after LAD ligation, with no significant change at 28 days (Fig. 1b). These results indicate that TRIM21 may play a role in the regulation of post-MI atrial remodeling. Next, a TRIM21 knockout mouse model was constructed to confirm the role of TRIM21 in MI-induced atrial remodeling. As shown in Fig. 1c, compared to mice in the WT-Sham group, WT-MI mice exhibited increased LA fibrosis, as demonstrated by the increased expression of the fiber-related proteins collagen I and α-SMA, whereas TRIM21 deficiency attenuated this fibrosis. Similar results were obtained using Masson's trichrome staining (Fig. 1d). Collectively, these data suggest that TRIM21 deficiency alleviates MI-induced atrial fibrosis.

3.2. TRIM21 deficiency mitigates LA enlargement

Echocardiography and electrocardiography were performed four weeks after MI, after which the mice were sacrificed. Fig. 2a shows a gross specimen of the LA. No morphological changes were observed in TRIM21-deficient mice compared to those in the WT-Sham group under normal conditions. The LA weight (LAW)/left tibia length (TL), which is a measure of LA enlargement, was significantly increased after MI; however, this effect was significantly reduced in TRIM21 knockout mice. WGA staining showed that MI led to atrial myocytes hypertrophy (increase in cross-sectional area), while TRIM21 knockout could inhibit atrial myocyte hypertrophy (Fig. 2b). LA area/TL, a marker of LA enlargement, was also measured using echocardiography, and KO-MI mice were found to have a lower LA area/TL ratio than WT-MI mice (Fig. 2c). Both WT-MI and KO-MI groups exhibited a decreased peak E/A ratio compared to the respective Sham groups, and there was no significant difference between the two MI groups (Fig. 2c). Furthermore, electrocardiogram parameters showed that the P-wave duration and PR interval were both significantly lengthened in the WT-MI groups, whereas TRIM21 ablation significantly inhibited these effects following MI (Fig. 2d). Overall, these results demonstrated that TRIM21 deficiency can mitigate MI-induced atrial enlargement.

3.3. TRIM21 ablation inhibits atrial myocyte apoptosis and Cx43 downregulation in the LA post-MI

Apoptosis of cardiomyocytes can lead to myocardial fibrosis [23]. Therefore, the effect of TRIM21 deficiency on atrial myocyte apoptosis following MI was evaluated by western blotting and TUNEL staining. As shown in Fig. 3a, MI resulted in increased DNA damage (evidenced by increased γ-H2AX expression) and cardiomyocyte apoptosis (as indicated by the decreased Bcl-2/Bax ratio) compared with the sham group. However, TRIM21 knockout significantly attenuated MI-induced injury and apoptosis. This was further corroborated by the TUNEL staining assay (Fig. 3b). Alterations in Cx43 expression correlated with atrial electrical remodeling [24]. The role of TRIM21 in Cx43 expression was further investigated by western blotting and immunofluorescence assays. The findings revealed that deletion of TRIM21 counteracted the MI-induced decline of Cx43 in mouse atrial tissues (Fig. 3a). This was further verified by immunofluorescence assays of atrial sections (Fig. 3c). Therefore, the findings suggest that TRIM21 deletion can reduce atrial myocyte apoptosis and Cx43 downregulation following MI.

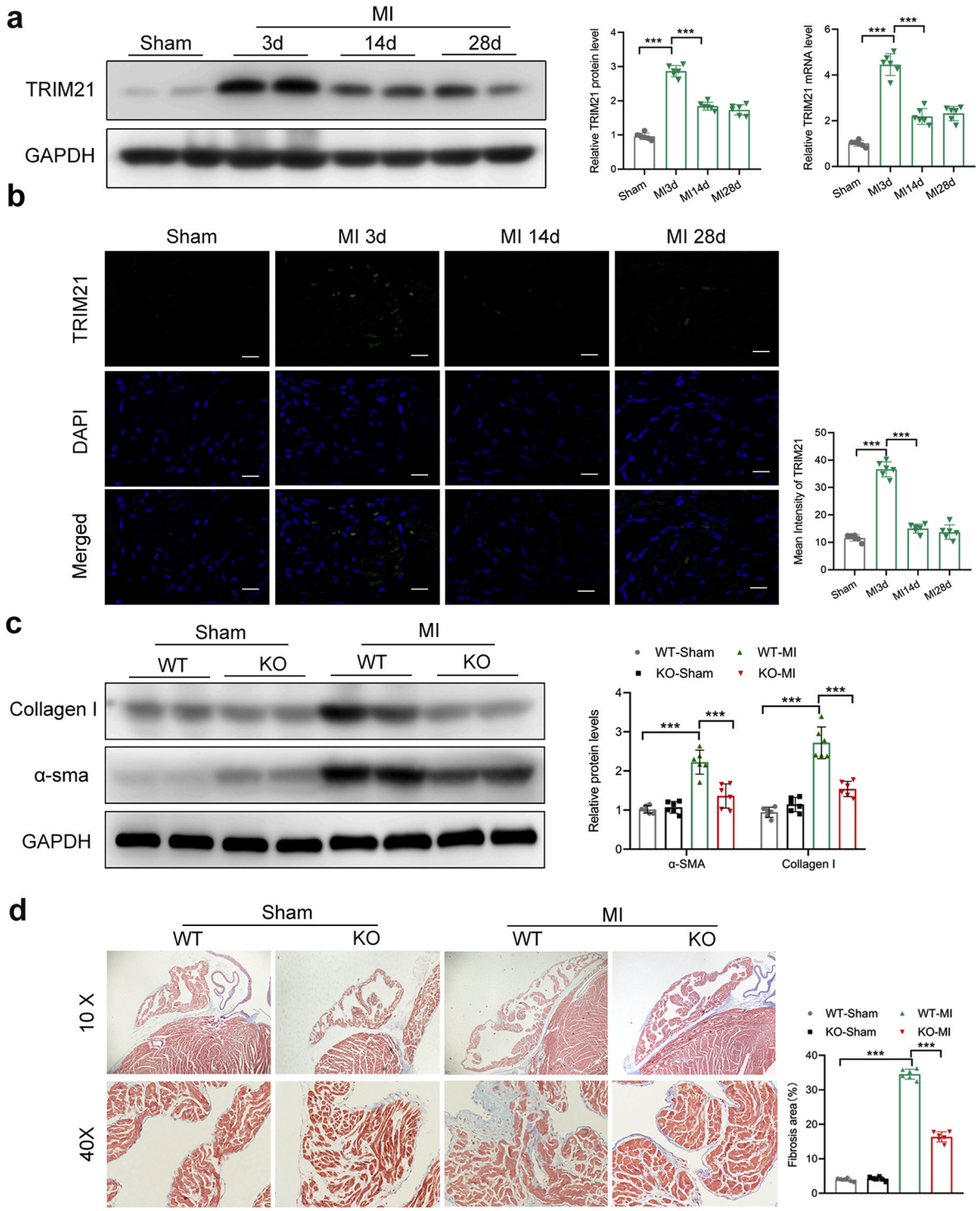

Fig. 1. TRIM21 deficiency alleviated left atrial fibrosis in mice post myocardial infarction. (a) Relative TRIM21 protein and mRNA levels in mouse LA at 3,14,28 days post-MI compared with the sham group. (b) Representative immunofluorescence of TRIM21 (green) and DAPI (blue) in the LA at 3,14,28 days (scale bar: 20 μm). Quantitative analysis of TRIM21 fluorescence intensity. (c) The protein levels of collagen I and α-SMA were measured by western blot analysis. Quantitative analysis of collagen I and α-SMA. (d) Representative images of left atrial tissues at 28 days post-MI stained with Masson trichrome. Quantitative analysis of LA fibrosis. *P < 0.05, **P < 0.01, ***P < 0.001. LA, left atrial; MI, myocardial infarction; DAPI, 4′, 6-diamidino-2-phenylindole. (For interpretation of the references to colour in this figure legend, the reader is referred to the Web version of this article.)

3.4. TRIM21 deficiency suppresses oxidative stress and inflammation in LA post-MI

Oxidative stress and inflammation are closely associated with atrial remodeling [7]. Therefore, the role of TRIM21 in MI-induced oxidative stress and inflammation was examined. TRIM21 deficiency led to an increase in the antioxidant enzyme SOD and a decline in the oxidative stress markers ROS and MDA in the atrial tissues post-MI (Fig. 4a). Additionally, TRIM21 depletion resulted in a significant decrease in MI-induced inflammation, as indicated by a reduction in macrophage infiltration (MAC-2-positive macrophages) and expression of proinflammatory factors (IL-1β and IL-6) (Fig. 4b). Taken together, these

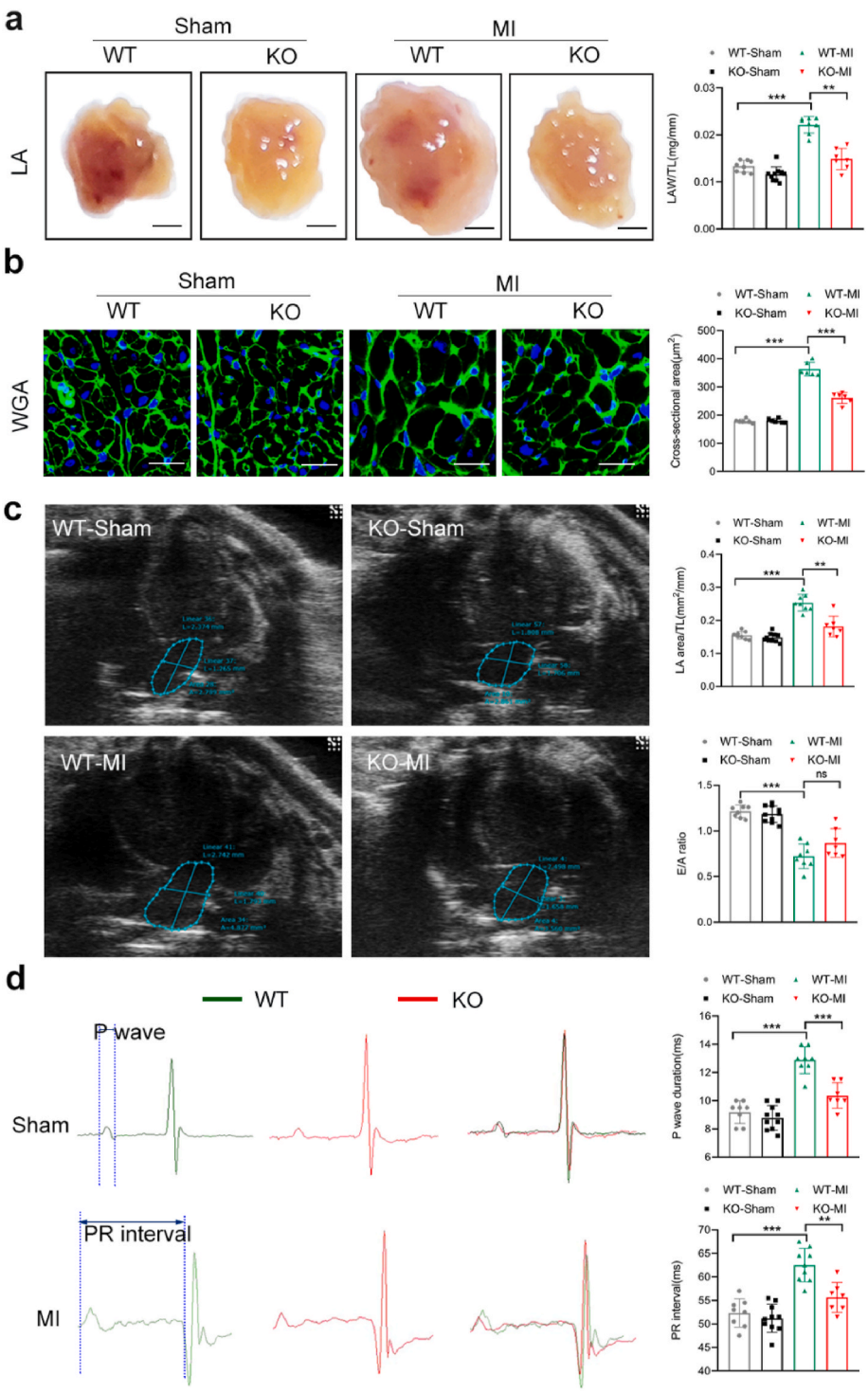

Fig. 2. TRIM21 deficiency moderated left atrial enlargement in mice post-MI. (a) The gross specimen of the LA at 28 days post-MI. Quantitative analysis of LAW/TL at 28 days post-MI. (b) Representative wheat germ agglutinin (WGA) immunofluorescence staining images (scale bar: 20 μm) and quantitative analyses of myocyte cross-sectional area. (c) Representative echocardiographic images at 28 days post-MI. Quantitative analysis of LA area/TL and E/A ratio. (d) Representative electrocardiograph images at 28 days post-MI. Quantitative analysis of P wave duration and PR interval. *P < 0.05, **P < 0.01, ***P < 0.001. LAW indicates left atrial weight; TL, tibia length.

findings suggest that the absence of TRIM21 mitigates MI-induced inflammation and oxidative stress in atrial tissues.

3.5. *TRIM21 overexpression exacerbates oxidative stress, cell apoptosis, and Cx43 downregulation induced by H_2O_2 in HL-1 cells*

Additional experiments were conducted to evaluate the influence of TRIM21 on oxidative stress, DNA damage, apoptosis, and Cx43 expression *in vitro*. A TRIM21 lentivirus (Lenti-TRIM21) was used to overexpress TRIM21 in HL-1 cells, and an empty vector lentivirus was used as a negative control (NC). The overexpression of TRIM21 was then verified through western blotting, quantitative reverse transcription-PCR, and immunofluorescence assays (Supplementary Fig. 1). The cells were divided into four groups: NC + PBS, Lenti-TRIM21 + PBS, NC + H_2O_2, and Lenti-TRIM21 + H_2O_2. As shown in Fig. 5a, H_2O_2 treatment caused a significant increase in ROS and MDA levels as well as a decrease in SOD antioxidant enzyme activity. In addition, TRIM21 overexpression further augmented ROS and MDA levels, as well as further decrease SOD activity following H_2O_2 exposure. Consequently, H_2O_2 treatment resulted in augmented oxidative damage in HL-1 cells (evidenced by increased γ-H2AX expression and a diminished Bcl-2/Bax ratio) and decreased Cx43 expression compared to that in the NC +

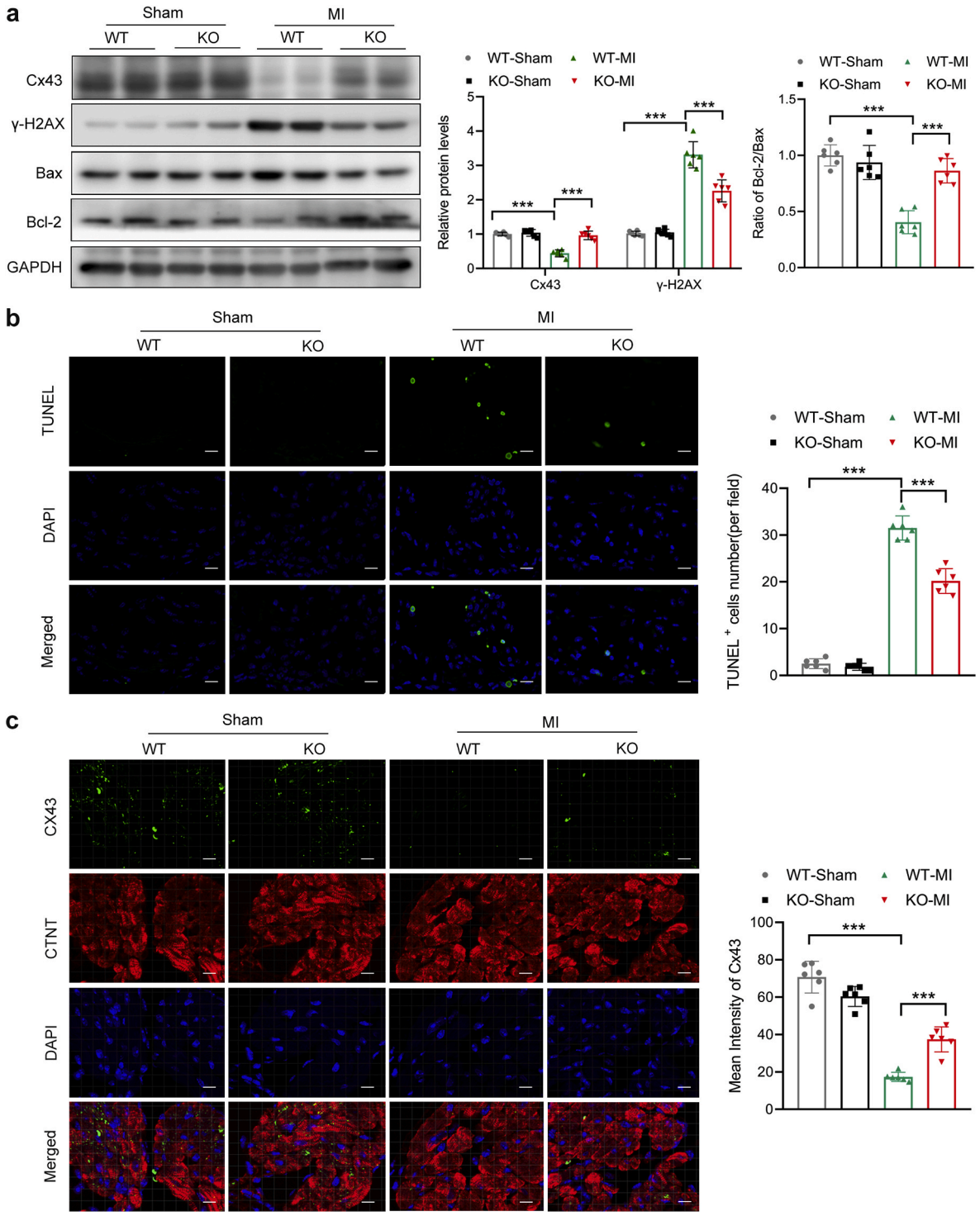

Fig. 3. TRIM21 deficiency inhibited MI-induced atrial myocyte apoptosis and Cx43 downregulation. (a) The protein levels of Cx43, Bcl-2, Bax and γ-H2AX were measured by western blot analysis. Quantitative analysis of Cx43, Bcl-2, Bax and γ-H2AX. (b) Representative immunofluorescence staining of TUNEL (green) and DAPI (blue) Quantitative analysis of TUNEL-positive cells. (c) Representative immunostaining images of Cx43 (green), CTNT (red) and DAPI (blue) in the LA at 3 days (scale bar: 20 μm). Quantitative analysis of Cx43 fluorescence intensity. *P < 0.05, **P < 0.01, ***P < 0.001. Cx43 indicates connexin 43; CTNT, cardiac troponin T; TUNEL: TdT-mediated dUTP-biotin nick end labeling; Bcl-2, B-cell CLL/lymphoma-2; Bax, Bcl-2-associated protein X. (For interpretation of the references to colour in this figure legend, the reader is referred to the Web version of this article.)

PBS group; TRIM21 overexpression further augmented oxidative damage and Cx43 downregulation in HL-1 cells exposed to H_2O_2 (Fig. 5b). In addition, TRIM21 overexpression increased the number of TUNEL-positive HL-1 cells exposed to H_2O_2 (Fig. 5c). Collectively, these findings suggest that TRIM21 plays a role in regulating oxidative stress, apoptosis, and Cx43 expression under stressful conditions.

3.6. *TRIM21 promotes cell apoptosis and Cx43 downregulation by inducing oxidative stress*

The ROS inhibitor NAC was used to investigate the correlation between TRIM21-induced apoptosis, Cx43 downregulation, and ROS production. HL-1 cells were divided into four different groups: NC +

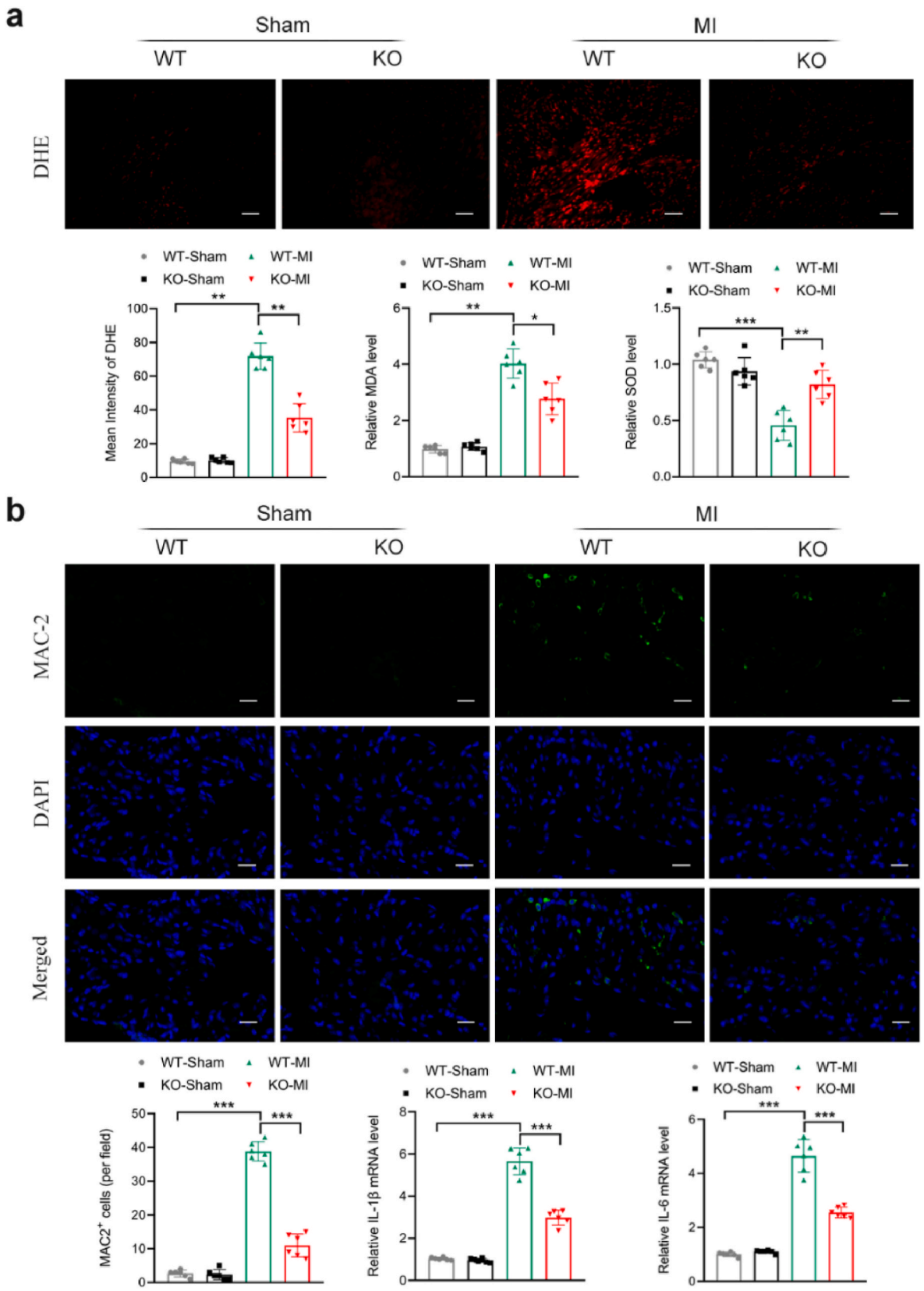

Fig. 4. TRIM21 deficiency attenuates MI-mediated oxidative stress and inflammation. (a) Representative immunofluorescence staining of DHE in the LA at 3 days (scale bar: 20 μm). Quantitative analysis of DHE fluorescence intensity. Quantitative analysis of relative MDA and SOD levels. (b). Representative immunofluorescence staining of MAC-2 (green) and DAPI (blue) in the LA at 3 days (scale bar: 20 μm). Quantitative analysis of MAC-2-positive cells. Relative IL-1β and IL-6 mRNA levels. *P < 0.05, **P < 0.01, ***P < 0.001. (For interpretation of the references to colour in this figure legend, the reader is referred to the Web version of this article.)

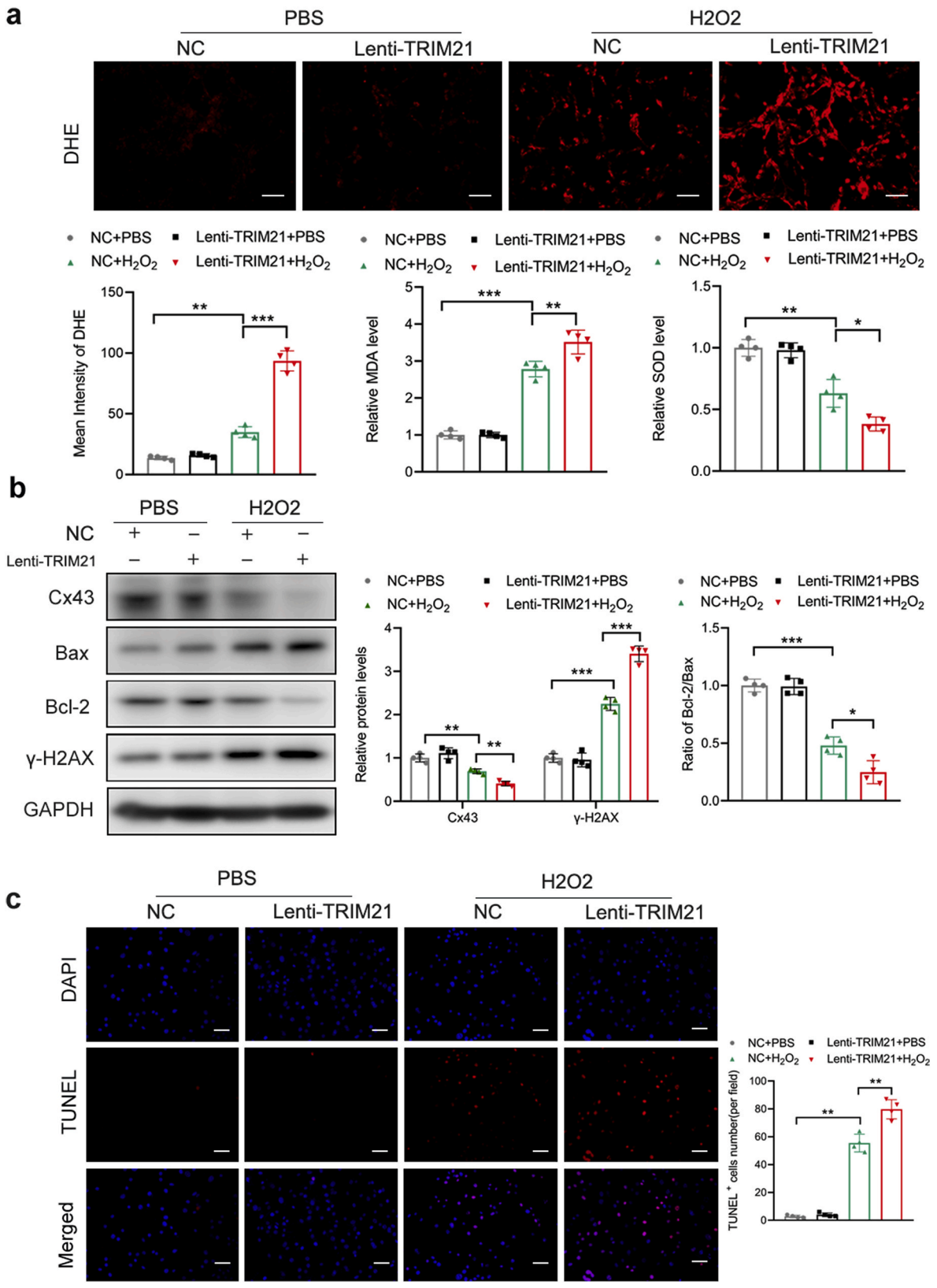

Fig. 5. TRIM21 overexpression aggravated oxidative stress, cell apoptosis, and Cx43 downregulation in HL-1 cells. HL-1 cells were transfected with lentivirus targeting the TRIM21 gene (Lenti-TRIM21) or negative control lentivirus (NC) and then treated with H_2O_2 or PBS. (A) Representative images of DHE staining in each group. Scale bar: 50 μm. Quantitative analysis of DHE fluorescence intensity. Quantitative analysis of relative MDA and SOD levels. (B) The protein levels of Cx43, Bcl-2, Bax and γ-H2AX were measured by western blot analysis. Quantitative analysis of Cx43, Bcl-2, Bax and γ-H2AX. (C) Representative immunofluorescence staining of TUNEL (red) and DAPI (blue) in each group. Scale bar: 50 μm. Quantitative analysis of TUNEL-positive cells. *P < 0.05, **P < 0.01, ***P < 0.001. PBS indicates phosphate-buffered saline; H_2O_2, hydrogen peroxide. (For interpretation of the references to colour in this figure legend, the reader is referred to the Web version of this article.)

DMSO + H_2O_2, NC + NAC + H_2O_2, Lenti-TRIM21 + DMSO + H_2O_2, and Lenti-TRIM21 + NAC + H_2O_2. NAC significantly decreased ROS and MDA levels and increased SOD activity compared to DMSO treatment (Fig. 6a). Consistent with this, the DNA damage- and apoptosis-promoting effects of TRIM21 overexpression were attenuated by NAC, as evidenced by the increased Bcl-2/Bax ratio and decreased γ-H2AX expression (Fig. 6b). NAC also reduced the number of TUNEL-positive HL-1 cells induced by TRIM21 overexpression (Fig. 6c). Furthermore, NAC pretreatment reversed the decrease in Cx43 expression caused by TRIM21 overexpression (Fig. 6b). These findings indicated that TRIM21 may promote HL-1 cell apoptosis and Cx43 downregulation by exacerbating ROS production and subsequent oxidative stress.

3.7. TRIM21 promotes oxidative stress, cell apoptosis and Cx43 downregulation by upregulating Nox2

NADPH oxidase enzymes are important sources of ROS in the cardiovascular system, and the main isoform expressed in the human atria is Nox2(10,11). Analysis of Nox2 expression in atrial tissues of mice three days post-MI revealed that TRIM21 deficiency inhibited its expression, as demonstrated by western blotting (Fig. 7a). Additionally, *in vitro* studies conducted on HL-1 cells exposed to H_2O_2 demonstrated that TRIM21 overexpression further upregulated Nox2 expression (Fig. 7b). These results suggest that Nox2 may play a role in TRIM21-mediated ROS production and oxidative stress. To test this hypothesis, the chemical compound Vas2870 was used to inhibit Nox2 activity. The cells were divided into four groups: NC + DMSO + H_2O_2, NC + Vas2870 + H_2O_2, Lenti-TRIM21 + DMSO + H_2O_2, and Lenti-TRIM21 + Vas2870 + H_2O_2. As shown in Fig. 7d, Vas2870 attenuated the oxidative stress caused by TRIM21 overexpression, which is indicated by increased SOD activity and decreased levels of ROS and MDA. Pretreatment with Vas2870 also inhibited TRIM21 overexpression-induced DNA damage, apoptosis, and Cx43 downregulation (Fig. 7c). Furthermore, the number of TUNEL-positive cells was also reduced in the Vas2870-treated group compared to that in the Lenti-TRIM21 + DMSO + H_2O_2 group (Fig. 7e). Taken together, these findings suggest that TRIM21 can induce apoptosis and oxidative stress and decrease Cx43 expression in atrial myocytes, at least partially through the upregulation of Nox2.

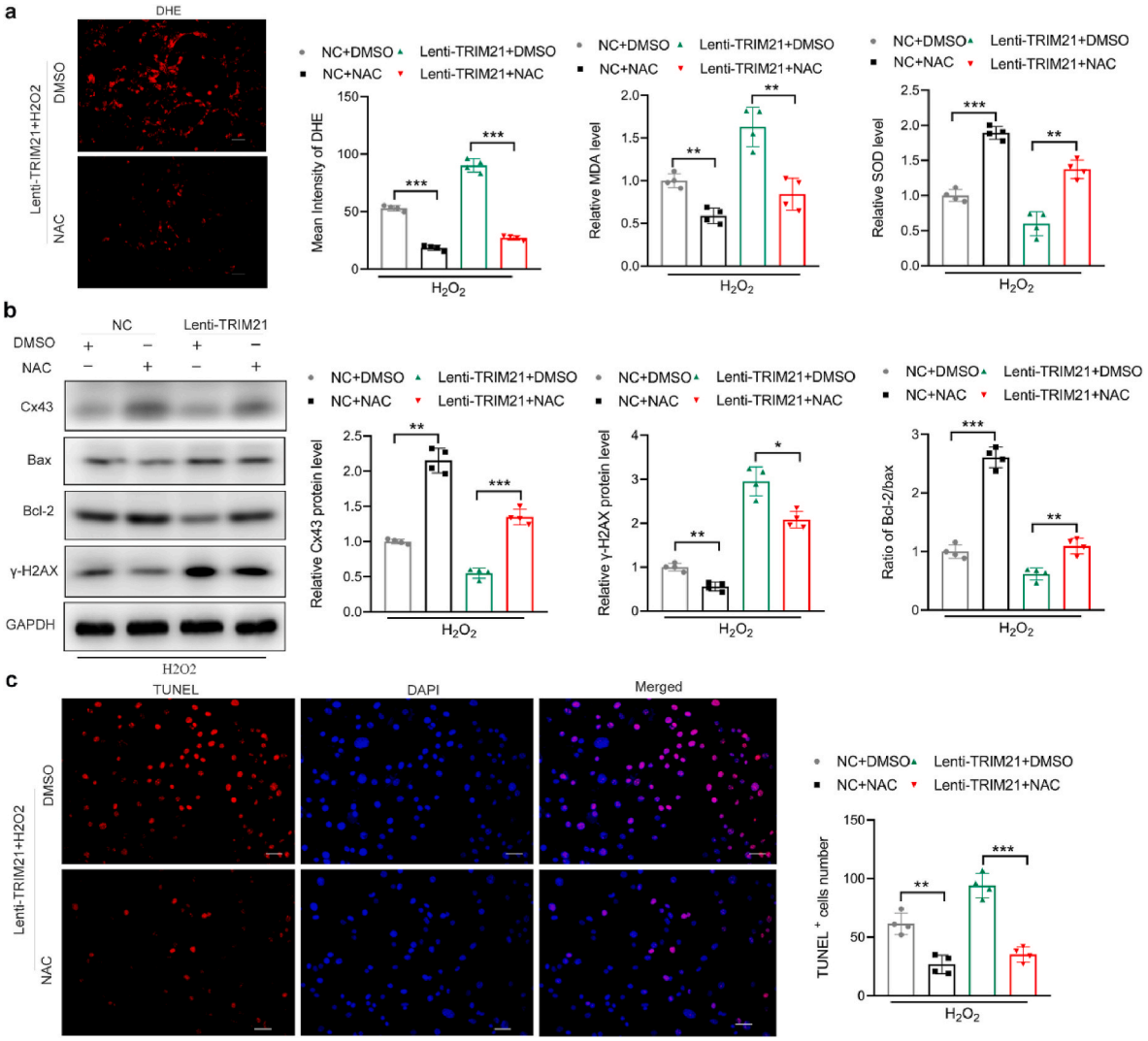

Fig. 6. NAC alleviated TRIM21 overexpression-induced oxidative damage and Cx43 downregulation. Cells were pretreated with NAC or DMSO before exposure to H_2O_2. (a) Representative images of DHE staining in each group. Scale bar: 50 μm. Quantitative analysis of DHE fluorescence intensity. Quantitative analysis of relative MDA and SOD levels. (b) The protein levels of p–NF–κB, t–NF–κB, Cx43, Bcl-2, Bax and γ-H2AX were measured by western blot analysis. Quantitative analysis of p–NF–κB/t–NF–κB, Cx43, Bcl-2, Bax and γ-H2AX. (c) Representative immunofluorescence staining of TUNEL (red) and DAPI (blue) in each group. Scale bar: 50 μm. Quantitative analysis of TUNEL-positive cells. *P < 0.05, **P < 0.01, ***P < 0.001. DMSO, dimethyl sulfoxide; NAC, N-acetylcysteine. (For interpretation of the references to colour in this figure legend, the reader is referred to the Web version of this article.)

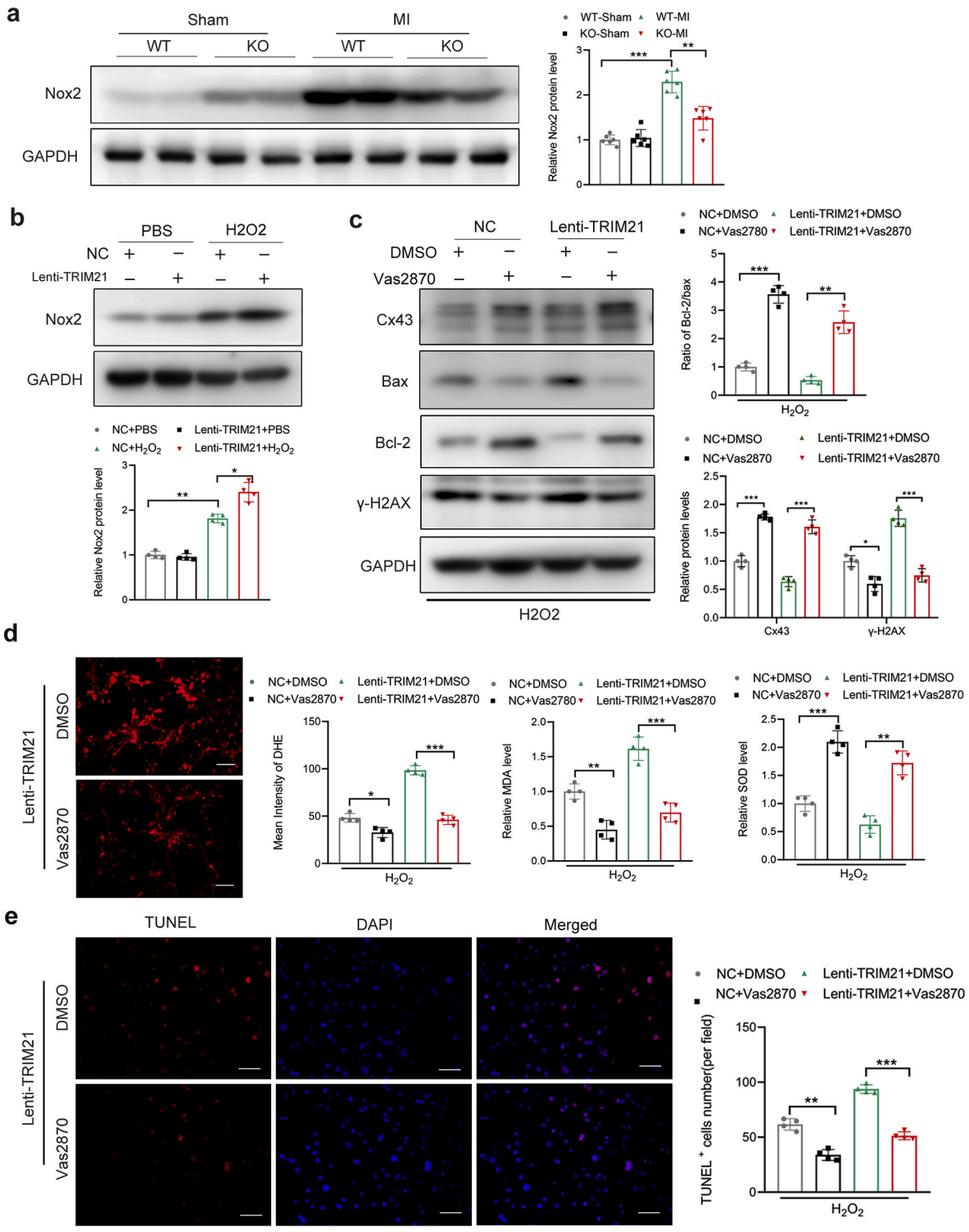

Fig. 7. Vas2870 alleviated TRIM21 overexpression-induced oxidative damage and Cx43 downregulation. Cells were pretreated with Vas2870 or DMSO before exposure to H_2O_2. (a) The protein levels of Nox2 in left atrium were measured by western blot analysis. Quantitative analysis of Nox2. (b) The protein levels of Nox2 in HL-1 cells were measured by western blot analysis. Quantitative analysis of Nox2. (c) The protein levels of Cx43, Bcl-2, Bax and γ-H2AX were measured by western blot analysis. Quantitative analysis of Cx43, Bcl-2, Bax and γ-H2AX. (d) Representative images of DHE staining in each group. Scale bar: 50 μm. Quantitative analysis of DHE fluorescence intensity. Quantitative analysis of relative MDA and SOD levels. (e) Representative immunofluorescence staining of TUNEL (red) and DAPI (blue) in each group. Scale bar: 50 μm. Quantitative analysis of TUNEL-positive cells. *P < 0.05, **P < 0.01, ***P < 0.001. DMSO, dimethyl sulfoxide. (For interpretation of the references to colour in this figure legend, the reader is referred to the Web version of this article.)

3.8. TRIM21 promotes oxidative stress and Nox2 expression by activating the NF-κB pathway

To gain further insight into the regulation of Nox2 by TRIM21, the role of the nuclear transcription factor was examined. Significant evidence indicates that Nox2 can be regulated by the nuclear transcription factor NF-κB [25,26]. Therefore, NF-κB activity in mouse atrial tissues after MI was assessed. Abolishment of TRIM21 inhibited the NF-κB pathway in the atrial tissue of mice three days post-MI, as revealed by a decrease in the p–NF–κB/t–NF–κB ratio (Fig. 8a). In addition, *in vitro* cell experiments showed that TRIM21 overexpression significantly amplified NF-κB activity in HL-1 cells exposed to H_2O_2 compared to that in the single stimulation group treated with H_2O_2 only (Fig. 8b). The role of the NF-κB pathway in TRIM21-induced Nox2 upregulation and ROS oxidative stress was investigated using the NF-κB inhibitor Bay11-7082. The cells were divided into four groups: NC + DMSO + H_2O_2, NC + Bay11-7082 + H_2O_2, Lenti-TRIM21 + DMSO + H_2O_2, and Lenti--TRIM21 + Bay11-7082 + H_2O_2. The results showed that Bay11-7082 suppressed NF-κB pathway activation induced by H_2O_2, as evidenced by the decrease in the p–NF–κB/t–NF–κB ratio (Fig. 8c). The findings showed that Bay11-7082 impeded the upregulation of Nox2 induced by H_2O_2 (Fig. 8c). As expected, Bay11-7082 reduced the oxidative stress caused by TRIM21 overexpression, as indicated by the decreased levels of ROS and MDA and increased activity of SOD (Fig. 8d). TRIM21 overexpression-induced DNA damage (manifested by reduced γ-H2AX expression), apoptosis (demonstrated by an elevated Bcl-2/Bax ratio), and Cx43 downregulation were also reversed by Bay11-7082 (Fig. 8c). The inhibitory effect of Bay11-7082 on H_2O_2-induced HL-1 cell apoptosis was also verified by TUNEL assay (Fig. 8e). In summary, these data indicate that TRIM21 promotes Nox2 expression and oxidative damage in atrial myocytes, likely through the NF-κB signaling pathway.

4. Discussion

The main finding of this study was that knockout of the E3 ligase TRIM21 mitigated MI-induced atrial remodeling. The expression of TRIM21 in the LA of the mouse MI model was markedly elevated. TRIM21 deficiency alleviated MI-induced atrial oxidative damage, Cx43 downregulation, atrial fibrosis and enlargement, and abnormalities in electrocardiogram parameters (prolongation of the P-wave and PR interval). Overexpression of TRIM21 in atrial myocyte HL-1 cells further enhanced oxidative damage and Cx43 downregulation. Mechanistically, it was shown that TRIM21 might promote atrial myocyte oxidative damage via the NF-κB/Nox2 pathway. These results suggest that TRIM21 is involved in the pathogenesis of atrial myocyte oxidative damage and atrial remodeling following MI and imply that targeting TRIM21 could be a viable therapeutic option for MI-related atrial fibrillation.

Previously, we reported that patients with AF post-MI are at an increased risk of ischemic stroke and heart failure [3,27]. This study aimed to explore the possible mechanisms underlying AF following MI and focused on the left atrium, as AF usually originates in this area [28]. Several studies have documented MI-induced unfavorable LA structural and electrophysiological changes, including atrial myocyte hypertrophy, atrial enlargement, interstitial fibrosis, and dysregulation of gap junctions, thereby facilitating AF initiation and maintenance [29–32]. This is consistent with observations made in this study that showed increased apoptosis of atrial myocytes and decreased expression of Cx43

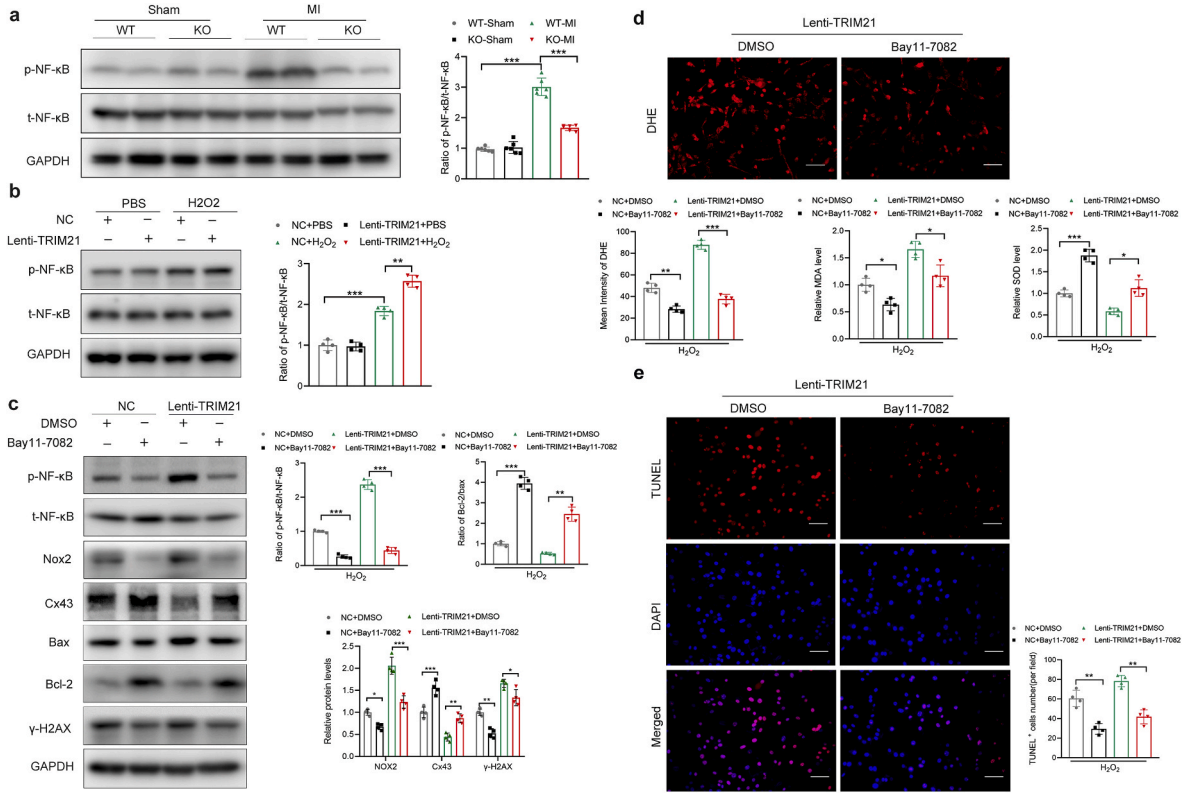

Fig. 8. Bay11-7082 inhibited TRIM21 overexpression-induced oxidative stress, cell apoptosis, and Cx43 downregulation. (a) The protein levels of p–NF–κB and t–NF–κB in LA were measured by western blot analysis. Quantitative analysis of p–NF–κB/t–NF–κB. Cells were pretreated with Bay11-7082 or DMSO before exposure to H_2O_2. (b) The protein levels of p–NF–κB and t–NF–κB in HL-1 cells were measured by western blot analysis. Quantitative analysis of p–NF–κB/t–NF–κB. (c) The protein levels of p–NF–κB, t–NF–κB, Cx43, Bcl-2, Bax and γ-H2AX were measured by western blot analysis. Quantitative analysis of p–NF–κB/t–NF–κB, Cx43, Bcl-2, Bax and γ-H2AX. (d) Representative images of DHE staining in each group. Scale bar: 50 μm. Quantitative analysis of DHE, MDA and SOD levels. (e) Representative immunofluorescence staining of TUNEL (red) and DAPI (blue) in each group. Scale bar: 50 μm. Quantitative analysis of TUNEL-positive cells. *P < 0.05, **P < 0.01, ***P < 0.001. (For interpretation of the references to colour in this figure legend, the reader is referred to the Web version of this article.)

in the left atria of mice in the early post-MI period, as well as marked atrial fibrosis and enlargement in the later stages.

Several factors are involved in atrial remodeling post-MI, including atrial ischemia, atrial stretch and enlargement, inflammation, ventricular dysfunction, and autonomic nervous system changes [6]. Recent studies have highlighted oxidative stress and inflammation as putative mediators of postmyocardial infarction atrial electrical and structural remodeling. For example, elevated levels of oxidative stress and inflammation biomarkers have been linked to the onset of AF in patients with ST elevation MI(7). Simvastatin mitigated oxidative stress and reduced susceptibility to AF in a rat model of ischemic heart failure [33]. In this study, it was found that mice suffering from MI exhibited increased oxidative stress, as indicated by increased levels of ROS and MDA and decreased SOD activity. TRIM21, an E3 ligase, was initially identified as a cytosolic IgG receptor that enables intracellular virus neutralization by antibodies [34]. Recent studies have revealed that TRIM21 is highly expressed in mammalian hearts and plays important roles in cardiovascular disease [14,16,17]. For example, TRIM21 is upregulated in the ventricle after MI and exacerbates myocardial injury by promoting M1 macrophage polarization [19]. TRIM21 loss attenuates TAC-induced myocyte oxidative damage by enhancing the Kelch-like ECH-associated protein 1 (Keap1)-nuclear factor erythroid 2-related factor 2 (Nrf2) antioxidant pathways [16]. This study found that TRIM21 expression in the mouse atria exhibited an increasing trend at an early stage after MI. Based on the above data, it was hypothesized that TRIM21 may be involved in postmyocardial infarction atrial remodeling.

Consistent with this hypothesis, TRIM21 knockout was found to mitigate postmyocardial infarction atrial structure remodeling, as demonstrated by reduced atrial fibrosis and enlargement. Atrial fibrosis can lead to intra- and interatrial conduction inhomogeneity, thus facilitating re-entry formation and contributing to AF occurrence and maintenance [35]. Left atrial enlargement is an independent predictor of incident AF in patients with MI(3). An epicardial mapping study showed that MI-induced structurally remodeled atria exhibit prolonged atrial activation times and slowed atrial conduction [36]. This study found that TRIM21 ablation alleviated MI-induced downregulation of Cx43, a vital gap junction protein in atrial myocytes that is essential for maintaining electrical conduction [24]. Low levels of Cx43 expression may lead to connexin remodeling and AF initiation [24,37]. The mechanism through which TRIM21 KO influences the expression of Cx43 remains unclear and may be related to increased oxidative stress and inflammation levels [37]. Changes in atrial electrophysiology and structure can be reflected in electrocardiographic parameters such as the PR interval representing atrial depolarization time and P-wave durations indicating atrial and atrioventricular nodal conduction [37,38]. This study showed that TRIM21 ablation significantly inhibited MI-induced P wave and PR interval prolongation. Overall, these results suggest that TRIM21 may promote postmyocardial infarction atrial remodeling and abnormal atrial electrical activity.

As TRIM21 is involved in regulating redox balance, it was speculated that TRIM21 promotes postmyocardial infarction atrial remodeling by aggravating oxidative stress. Here, it was shown that TRIM21 KO mice exhibited attenuated oxidative stress levels in LA tissues after MI, as manifested by decreased ROS and MDA levels and increased SOD levels. Moreover, TRIM21 ablation attenuates MI-induced oxidative injury in atrial myocytes by inhibiting apoptosis and DNA damage. This finding was confirmed with *in vitro* experiments. TRIM21 overexpression in HL-1 cells led to augmented oxidative damage and apoptosis following exposure to H_2O_2. Furthermore, NAC was used to eliminate ROS production, and NAC was found to reverse HL-1 cell DNA damage and apoptosis induced by TRIM21 overexpression. This indicates that TRIM21 promotes stress-induced atrial myocyte apoptosis by enhancing oxidative stress. Notably, oxidative stress and inflammation are highly intertwined [39,40]. Analysis of inflammatory markers in atrial tissues showed that TRIM21 KO diminished LA macrophage infiltration (MAC-2-positive cells) and inhibited the expression of proinflammatory cytokines (IL-1β and IL-6) after MI. From this, it is suggested that TRIM21 might promote postmyocardial infarction atrial remodeling by aggregating atrial myocyte oxidative damage and amplifying inflammation.

Recent studies have reported a mechanism by which TRIM21 regulates oxidative stress. For example, TRIM21 exacerbates pressure overload-induced heart oxidative damage by promoting p62 ubiquitination, thereby impairing the Keap1-Nrf2 antioxidant pathway [41]. In this study, it was found that TRIM21 promotes the expression of Nox2, which is the main source of ROS generation in atrial myocytes. Nox2 is markedly upregulated in atrial tissues from animal models and patients with AF(10,11). Mighiu et al. demonstrated that increased Nox2 expression in mice leads to higher levels of superoxide production and heightened susceptibility to AF [42]. Therefore, it was speculated that TRIM21 may promote atrial oxidative stress following MI by upregulating Nox2, thus facilitating myocardial oxidative damage. The pro-oxidative stress effect of TRIM21 was found to be inhibited by the Nox2 inhibitor Vas2870. These findings demonstrate that Vas2870 treatment can successfully reduce oxidative damage, apoptosis, and Cx43 downregulation caused by the overexpression of TRIM21 in HL-1 cells. This indicates a Nox2-dependent mechanism by which TRIM21 controls oxidative stress.

Additionally, further explored was the potential mechanism by which TRIM21 regulates the expression of Nox2. NF-κB was recently shown to promote ROS production and oxidative stress by inducing the expression of genes such as NADPH oxidase Nox2(25,26). Other studies have found that TRIM21 promotes the activation of the NF-κB pathway. Deletion of TRIM21 suppresses M1 microglial polarization through the NF-κB/NLR family pyrin domain-containing 3 inflammasome pathway [43]. TRIM21 deficiency in mice impedes the expression of NF-κB downstream proinflammatory genes [44,45]. Our results are consistent with these observations; TRIM21 deficiency hindered NF-κB activation in the left atrium of mice following MI, whereas its overexpression in HL-1 cells exposed to H_2O_2 further amplified NF-κB activation. TRIM21 may regulate NF-κB activity through multiple mechanisms: enhancing the interaction between NF-κB and IB kinase via ubiquitination of NF-κB subunits, ubiquitinating and degrading of prohibitin 1, a repressor of the NF-κB pathway, and targeting different members in NF-κB signaling, including Transforming growth factor beta-activated kinase 1 (TAK1), IκB kinase-α (IKKα), and IκB1 [46–48]. To ascertain whether TRIM21 induces Nox2 upregulation through the NF-κB pathway, the NF-κB inhibitor Bay11-7082 was used. The results showed that Bay11-7082 effectively inhibited TRIM21 overexpression-induced Nox2 upregulation and atrial myocyte oxidative damage. Overall, the data suggest that TRIM21 promotes nox2 expression and oxidative stress, possibly via the NF-κB pathway (Fig. 9).

This study suggests that TRIM21 deficiency could be beneficial in protecting against atrial inflammation and pathological remodeling that occur after MI. The mechanism of this protection may be linked to the NF-κB/Nox2 pathway and the reduction in oxidative stress. These findings provide a potential target for preventing atrial remodeling following MI, which is of immense significance in both the research and clinical realms.

5. Study limitations

In this study, we demonstrated the role of TRIM21 in post myocardial infarction atrial pathological remodeling. We have previously established a mouse model of atrial fibrillation and the incidence was recorded. The incidences of atrial fibrillation in WT-MI group and the KO-was 30% (3/10) and 20% (2/10), respectively. The induction rate of atrial fibrillation in mice seemed relatively low, thus the effects of TRIM21 on the incidence and duration of AF still require further investigation.

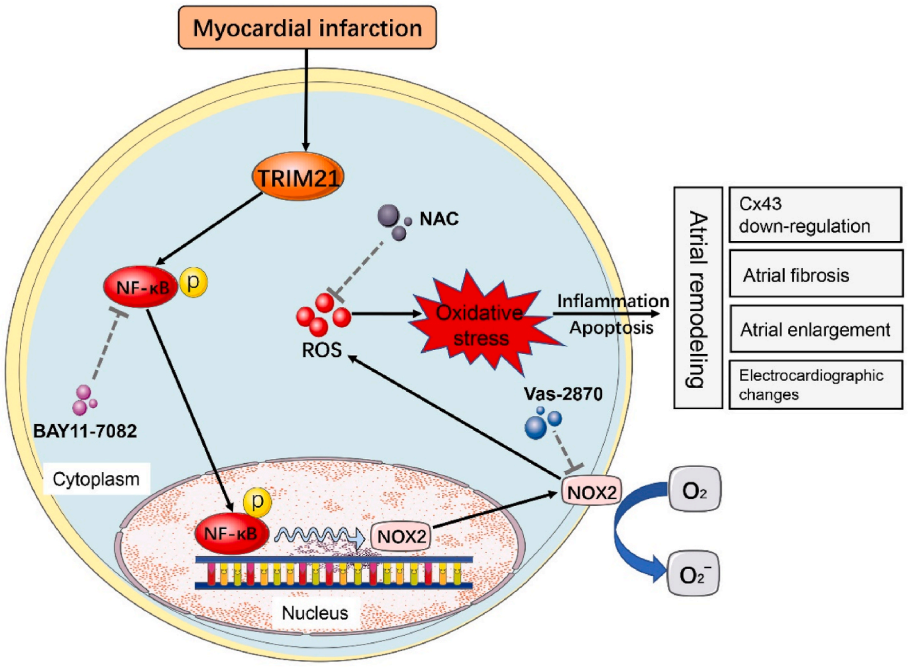

Fig. 9. Schematic diagram illustrating that TRIM21 promotes atrial remodeling post myocardial infarction by attenuating oxidative stress and inflammation via the NF-κB signaling pathway. TRIM21 triggers NF-κB signaling pathway activation, thus promoting Nox2 expression. The upregulation of Nox2 can further contribute to ROS production, oxidative damage and inflammation, which eventually leads to atrial remodeling.

Author contributions

Yidong Wei and Xiangdong Liu designed this study. Xiangdong Liu, Wenming Zhang, and Xingxu Zhang conducted experiments. Jiacheng Luo analyzed the data. Xiangdong Liu wrote the manuscript. Yidong Wei and Baoxin Liu revised the manuscript accordingly. All authors have read and approved the final manuscript.

Ethics statement

All animal protocols were approved by the Ethics Committee of Shanghai Tenth People's Hospital of Tongji University School of Medicine (approval number: SHDSYY-2020-1734), following the Care and Use of Medical Laboratory Animals Guidelines (Ministry of Health, P. R. China, 1998).

Funding

This work was supported by the Shanghai Sailing Program [No. 19YF1437900], the Climbing Program of Shanghai Tenth People's Hospital [No. 2021SYPDRC035], the National Natural Science Foundation of China [No. 81900385] to Dr. Baoxin Liu, the Natural Science Foundation of Shanghai [Grant No. 18ZR1429700] and the National Natural Science Foundation of China [Grant No. 81270193] to Dr. Yidong Wei, and the National Natural Science Foundation of China [No. 82200318] to Dr. Jiacheng Luo.

Declaration of competing interest

The authors declare that they have no known competing financial interests or personal relationships that could have appeared to influence the work reported in this paper.

Data availability

Data will be made available on request.

Acknowledgments

We would like to thank Zhanju Liu (Department of Gastroenterology, Shanghai Tenth People's Hospital of Tongji University School of Medicine) for providing TRIM21 knockout mice.

Appendix A. Supplementary data

Supplementary data to this article can be found online at https://doi.org/10.1016/j.redox.2023.102679.

References

[1] A. Romanov, M. Martinek, H. Pürerfellner, et al., Incidence of atrial fibrillation detected by continuous rhythm monitoring after acute myocardial infarction in patients with preserved left ventricular ejection fraction: results of the ARREST study, EP Europace 20 (2018) 263–270.
[2] J. Schmitt, G. Duray, B.J. Gersh, S.H. Hohnloser, Atrial fibrillation in acute myocardial infarction: a systematic review of the incidence, clinical features and prognostic implications, Eur. Heart J. 30 (2009) 1038–1045.
[3] J. Luo, S. Xu, H. Li, et al., Long-term impact of new-onset atrial fibrillation complicating acute myocardial infarction on heart failure, ESC.Heart Fail. 7 (2020) 2762–2772.
[4] B.S. Crenshaw, S.R. Ward, C.B. Granger, et al., Atrial fibrillation in the setting of acute myocardial infarction: the GUSTO-I experience, J. Am. Coll. Cardiol. 30 (1997) 406–413.
[5] B.A. Schoonderwoerd, I.C. Van Gelder, D.J. Van Veldhuisen, M.P. Van den Berg, H. J. Crijns, Electrical and structural remodeling: role in the genesis and maintenance of atrial fibrillation, Prog. Cardiovasc. Dis. 48 (2005) 153–168.
[6] J. Wang, Y.-M. Yang, J. Zhu, Mechanisms of new-onset atrial fibrillation complicating acute coronary syndrome, Herz 40 (2015) 18–26.
[7] H.A. Bas, F. Aksoy, A. Icli, et al., The association of plasma oxidative status and inflammation with the development of atrial fibrillation in patients presenting with ST elevation myocardial infarction, Scand. J. Clin. Lab. Investig. 77 (2017) 77–82.
[8] M.D. Bagatini, C.C. Martins, V. Battisti, et al., Oxidative stress versus antioxidant defenses in patients with acute myocardial infarction, Heart Ves. 26 (2011) 55–63.
[9] Y.H. Looi, D.J. Grieve, A. Siva, et al., Involvement of Nox2 NADPH oxidase in adverse cardiac remodeling after myocardial infarction, Hypertens. 51 (2008) 319–325.
[10] Y.M. Kim, T.J. Guzik, Y.H. Zhang, et al., A myocardial Nox2 containing NAD (P) H oxidase contributes to oxidative stress in human atrial fibrillation, Circ. Res. 97 (2005) 629–636.

[11] S.N. Reilly, R. Jayaram, K. Nahar, et al., Atrial sources of reactive oxygen species vary with the duration and substrate of atrial fibrillation: implications for the antiarrhythmic effect of statins, Circulation 124 (2011) 1107–1117.
[12] S. Yoo, A. Pfenniger, J. Hoffman, et al., Attenuation of oxidative injury with targeted expression of NOX2 shRNA prevents onset and maintenance of electrical remodeling in the canine atrium–a novel gene therapy approach to atrial fibrillation, Circulation 142 (2020) 1261.
[13] J.-P. Chang, M.-C. Chen, W.-H. Liu, et al., Atrial myocardial nox2 containing NADPH oxidase activity contribution to oxidative stress in mitral regurgitation: potential mechanism for atrial remodeling, Cardiovasc. Pathol. 20 (2011) 99–106.
[14] F. Wang, Y. Zhang, J. Shen, et al., The ubiquitin E3 ligase TRIM21 promotes hepatocarcinogenesis by suppressing the p62-Keap1-Nrf2 antioxidant pathway, Cellular and molecular gastroenterology and hepatology 11 (2021) 1369–1385.
[15] G. Zhou, H. Wu, J. Lin, R. Lin, B. Feng, Z. Liu, TRIM21 is decreased in Colitis-associated cancer and negatively regulates epithelial carcinogenesis, Inflamm. Bowel Dis. 27 (2021) 458–468.
[16] J.-A. Pan, Y. Sun, Y.-P. Jiang, et al., TRIM21 ubiquitylates SQSTM1/p62 and suppresses protein sequestration to regulate redox homeostasis, Mol. Cell 61 (2016) 720–733.
[17] M. Sjöstrand, B. Carow, W.A. Nyberg, R. Covacu, M.E. Rottenberg, A. Espinosa, TRIM21 controls toll-like receptor 2 responses in bone-marrow-derived macrophages, Immunology 159 (2020) 335–343.
[18] H. Liu, M. Li, Y. Song, W. Xu, TRIM21 restricts Coxsackievirus B3 replication, cardiac and pancreatic injury via interacting with MAVS and positively regulating IRF3-mediated type-I interferon production, Front. Immunol. 9 (2018) 2479.
[19] Z. Li, X. Liu, X. Zhang, et al., 8e polarization, Front. Immunol. 13 (2022), 1053171.
[20] E. Gao, Y.H. Lei, X. Shang, et al., A novel and efficient model of coronary artery ligation and myocardial infarction in the mouse, Circ. Res. 107 (2010) 1445–1453.
[21] D. Boulghobra, P.-E. Grillet, M. Laguerre, et al., Sinapine, but not sinapic acid, counteracts mitochondrial oxidative stress in cardiomyocytes, Redox Biol. 34 (2020), 101554.
[22] W. Han, C. Du, Y. Zhu, et al., Targeting myocardial mitochondria-STING-polyamine axis prevents cardiac hypertrophy in chronic kidney disease, Baic. Transl. Sci. 7 (2022) 820–840.
[23] P. Kong, P. Christia, N.G. Frangogiannis, The pathogenesis of cardiac fibrosis, Cell. Mol. Life Sci. 71 (2014) 549–574.
[24] X. Lin, J. Gemel, A. Glass, C.W. Zemlin, E.C. Beyer, R.D. Veenstra, Connexin40 and connexin43 determine gating properties of atrial gap junction channels, J. Mol. Cellular Cardiol. 48 (2010) 238–245.
[25] Y. Wang, H. Hu, J. Yin, et al., TLR4 participates in sympathetic hyperactivity Post-MI in the PVN by regulating NF-κB pathway and ROS production, Redox Biol. 24 (2019), 101186.
[26] J. Anrather, G. Racchumi, C. Iadecola, NF-κB regulates phagocytic NADPH oxidase by inducing the expression of gp91phox, J. Biol. Chem. 281 (2006) 5657–5667.
[27] J. Luo, S. Xu, H. Li, et al., Long-term impact of the burden of new-onset atrial fibrillation in patients with acute myocardial infarction: results from the NOAFCAMI-SH registry, EP Europace 23 (2021) 196–204.
[28] Oral Hakan, Post-operative atrial fibrillation and oxidative stress: a novel causal mechanism or another biochemical epiphenomenon? - ScienceDirect, J. Am. Coll. Cardiol. 51 (2008) 75–76.
[29] H.J. Hwang, J.-W. Ha, B. Joung, et al., Relation of inflammation and left atrial remodeling in atrial fibrillation occurring in early phase of acute myocardial infarction, Int. J. Cardiol. 146 (2011) 28–31.
[30] W. Hanif, L. Alex, Y. Su, et al., Left atrial remodeling, hypertrophy, and fibrosis in mouse models of heart failure, Cardiovasc. Pathol. 30 (2017) 27–37.
[31] M. Hohl, K. Erb, L. Lang, et al., Cathepsin A mediates ventricular remote remodeling and atrial cardiomyopathy in rats with ventricular ischemia/reperfusion, JACC (J. Am. Coll. Cardiol.): Baic.Transl. Sci. 4 (2019) 332–344.
[32] M. Liu, W. Li, H. Wang, et al., CTRP9 ameliorates atrial inflammation, fibrosis, and vulnerability to atrial fibrillation in post-myocardial infarction rats, J. Am. Heart Assoc. 8 (2019), e013133.
[33] K.-I. Cho, S.-H. Koo, T.-J. Cha, et al., Simvastatin attenuates the oxidative stress, endothelial thrombogenicity and the inducibility of atrial fibrillation in a rat model of ischemic heart failure, Int. J. Mol. Sci. 15 (2014) 14803–14818.
[34] D.L. Mallery, W.A. McEwan, S.R. Bidgood, G.J. Towers, C.M. Johnson, L.C. James, Antibodies mediate intracellular immunity through tripartite motif-containing 21 (TRIM21), Proc. Natl. Acad. Sci. USA 107 (2010) 19985–19990.
[35] X. He, X. Gao, L. Peng, et al., Atrial fibrillation induces myocardial fibrosis through angiotensin II type 1 receptor-specific Arkadia-mediated downregulation of Smad7, Circ. Res. 108 (2011) 164–175.
[36] M. Hohl, K. Erb, L. Lang, et al., Cathepsin A mediates ventricular remote remodeling and atrial cardiomyopathy in rats with ventricular ischemia/reperfusion, JACC Basic Transl Sci 4 (2019) 332–344.
[37] P. Hegner, S. Lebek, M. Tafelmeier, et al., Sleep-disordered breathing is independently associated with reduced atrial connexin 43 expression, Heart Rhythm 18 (2021) 2187–2194.
[38] I.A. Polejaeva, R. Ranjan, C.J. Davies, et al., Increased susceptibility to atrial fibrillation secondary to atrial fibrosis in transgenic goats expressing transforming growth factor-β1, J. Cardiovascular Electrophysiol. 27 (2016) 1220–1229.
[39] N. Khaper, S. Bryan, S. Dhingra, et al., Targeting the vicious inflammation–oxidative stress cycle for the management of heart failure, Antioxidants Redox Signal. 13 (2010) 1033–1049.
[40] P. Zhang, Y. Yin, T. Wang, et al., Maresin 1 mitigates concanavalin A-induced acute liver injury in mice by inhibiting ROS-mediated activation of NF-κB signaling, Free Radic. Biol. Med. 147 (2020) 23–36.
[41] K. Hou, J. Shen, J. Yan, et al., Loss of TRIM21 alleviates cardiotoxicity by suppressing ferroptosis induced by the chemotherapeutic agent doxorubicin, EBioMedicine 69 (2021), 103456.
[42] A.S. Mighiu, A. Recalde, K. Ziberna, et al., Inducibility, but not stability, of atrial fibrillation is increased by NOX2 overexpression in mice, Cardiovasc. Res. 117 (2021) 2354–2364.
[43] T. Xiao, J. Wan, H. Qu, Y. Li, Tripartite-motif protein 21 knockdown extenuates LPS-triggered neurotoxicity by inhibiting microglial M1 polarization via suppressing NF-κB-mediated NLRP3 inflammasome activation, Arch. Biochem. Biophys. 706 (2021), 108918.
[44] A. Espinosa, V. Dardalhon, S. Brauner, et al., Loss of the lupus autoantigen Ro52/Trim21 induces tissue inflammation and systemic autoimmunity by disregulating the IL-23–Th17 pathway, J. Exp. Med. 206 (2009) 1661–1671.
[45] R. Yoshimi, T.-H. Chang, H. Wang, T. Atsumi, H.C. Morse, K. Ozato, Gene disruption study reveals a nonredundant role for TRIM21/Ro52 in NF-κB-dependent cytokine expression in fibroblasts, J. Immunol. 182 (2009) 7527–7538.
[46] H. Wang, Y. Zhou, L. Oyang, et al., LPLUNC1 stabilises PHB1 by counteracting TRIM21-mediated ubiquitination to inhibit NF-κB activity in nasopharyngeal carcinoma, Oncogene 38 (2019) 5062–5075.
[47] L. Yang, T. Zhang, C. Zhang, C. Xiao, X. Bai, G. Wang, Upregulated E3 ligase tripartite motif-containing protein 21 in psoriatic epidermis ubiquitylates nuclear factor-κB p65 subunit and promotes inflammation in keratinocytes, Br. J. Dermatol. 184 (2021) 111–122.
[48] W.A. McEwan, J.C. Tam, R.E. Watkinson, S.R. Bidgood, D.L. Mallery, L.C. James, Intracellular antibody-bound pathogens stimulate immune signaling via the Fc receptor TRIM21, Nat. Immunol. 14 (2013) 327–336.